Communication

Safeguarding Cork's Beauty and Longevity: Innovations in Deposition of Protective Thin Films

Belgacem Tiss [1,*], Diego Martínez-Martínez [1,2], Catalina Mansilla [3], Joel Borges [1], Martin Andritschky [1] and Luís Cunha [1]

[1] Physics Center of Minho and Porto Universities (CF-UM-UP), Campus de Gualtar, 4710-057 Braga, Portugal; diegus.m2@gmail.com (D.M.-M.); joelborges@fisica.uminho.pt (J.B.); martin.andritschky@fisica.uminho.pt (M.A.); lcunha@fisica.uminho.pt (L.C.)

[2] Luxembourg Institute of Science and Technology, Esch-sur-Alzette, 4362 Luxembourg, Luxembourg

[3] CTECHnano Coatings Technologies S.L., Tolosa Hiribidea 76, 20018 San Sebastián, Spain; c.mansilla@ctechnano.com

[*] Correspondence: sofian.tis15@gmail.com or btiss@fisica.uminho.pt

Abstract: Cork is a sustainable natural material widely used as a wine stopper. However, some other uses, such as wall coverings, flooring, bags and shoes, face UV damage. To mitigate this issue, we explored the deposition of TiO_2 and ZnO thin films via magnetron sputtering on glass and cork substrates. Both films displayed uniformity and the lack of any discernible cracks or voids, remained transparent in the visible region, and offered UV protection. Thus, TiO_2 and ZnO blocked UV light with a wavelength of up to 310 nm ($E_g = 4$ eV) and 370 nm ($E_g = 3.3$ eV), respectively. Exposure tests, under a sun simulator lamp, revealed that the uncoated cork showed noticeable color changes, even when located under a glass substrate. The TiO_2 coating did not prevent cork discoloration, while ZnO prevented it. This study highlights ZnO thin films as a durable solution to safeguard cork materials from UV damage and extend their usability.

Keywords: cork; magnetron sputtering; TiO_2; ZnO; sun simulator; UV protection

1. Introduction

The incorporation of cork in various commonplace applications is a well-established practice, leveraging its unique properties. Despite its widespread use, certain applications continue to depend on the utilization of durable synthetic polymeric materials, often posing environmental concerns. As the demand for sustainable alternatives grows, it becomes imperative to reassess and expand the scope of cork applications, exploring its potential in areas traditionally dominated by synthetic materials. By doing so, environmentally friendly practices are promoted but also novel possibilities for the integration of cork in diverse industries are unlocked, contributing to a more sustainable and ecologically conscious future. Cork, as a renewable natural resource, offers a potential alternative to replace these synthetic materials in numerous common daily applications. The success of the substitution of synthetic environmentally unfriendly materials with cork has great transformative potential, including in the field of investigating ways of enhancing the longevity of cork, particularly when utilized in outdoor settings. Thereby it may promote a substantial and meaningful contribution to overall sustainability. This paradigm shift not only underscores the eco-friendly attributes of cork but also envisions a future where this versatile material becomes a preferred choice, aligning with the principles of environmental responsibility and resource conservation in diverse applications.

Cork is a natural material renowned for its distinct properties, which include excellent thermal and acoustic insulation, low gas and liquid permeability, high elasticity, low density, and substantial porosity [1,2]. Moreover, owing to its intricate morphology and chemical composition, cork possesses a unique set of properties, including a pronounced

hydrophobic character, chemical stability, and resistance to microbiological influences [3,4]. This combination of structural resilience and chemical attributes further enhances cork's suitability for various applications, making it not only a preferred choice for thermal and acoustic insulation but also a material of choice where resistance to moisture, chemicals, and microbiological factors is important [5,6] Notably, cork stands out as the only natural material with a Poisson coefficient very close to zero, earning it the moniker of a "zero Poisson ratio" [2,7]. These unique characteristics enable cork to find versatile applications beyond its traditional use as a wine stopper [8]. It is also employed in diverse areas such as flooring, SpaceX rockets, and wall construction to provide effective thermal and acoustic insulation [9,10]. Currently, cork production worldwide exceeds 300,000 to 350,000 tons annually, equating to nearly 20 million tons of steel in terms of volume [1,11]. This comparative analysis serves as a powerful tool to underscore not only the scale but also the remarkable significance of cork production on a global level. It effectively communicates the sheer magnitude of cork's presence and its role as a renewable and eco-friendly resource, contributing to a deeper understanding of its importance in the broader global context. But to allow the use of cork in a particular type of applications, this material has to be enriched to accomplish the task successfully. Previous studies on this subject include a review on cork composites [12] and references studying cork composites for specific applications, namely the influence of polyurethane (U030) as a cork grain adhesive on the thermal insulation properties, flexibility, and mechanical properties of the RC16 cork [13], cork–rubber composites' dynamic behavior, namely in vibration isolation applications [14–17], a natural cork/potato periderm for use in elastomer composites for energy absorption [18], and other cork-based composites, seeking to understand their ability to store electrical charge [19], to mention a few. However, when cork is exposed to sunlight, it suffers from rapid ageing and discoloration due to the influence of ultraviolet (UV) radiation from the sun [1]. This exposure adversely affects several key properties of cork, including its structural integrity, flexibility, and esthetic appeal. The impact of UV radiation can lead to the degradation of cork, including cork's natural polymers, resulting in a compromised texture and diminished strength. Additionally, discoloration occurs as a consequence of chemical changes within the cork components, diminishing its visual appeal and potentially limiting its applications. The mechanisms of photo- and thermal-aging in elastomers have been extensively documented in the literature [20,21], elucidating the formation of alkyl radicals and conjugate carbonyls. To ensure the durability of these materials within their operational environment, an interesting strategy entails the application of thin protective films. These films serve the dual purpose of shielding the materials from external stressors while preserving their inherent characteristics, particularly their color and visual appeal. Transparent metallic oxide films, such as titanium dioxide (TiO_2) and zinc oxide (ZnO), appear as noteworthy choices for that purpose. Both of these materials possess the unique property of transparency within the visible spectrum, coupled with opaqueness in the UV range [22–24]. Consequently, both TiO_2 and ZnO thin films have been explored for their utility as protective coatings for various applications. Johansson et al. [25] investigated transparent ZnO and TiO_2 thin films on PV cover glass. The ZnO coating shifted the optical bandgap, reducing destructive UV radiation transmittance by up to ~85%. In addition, Yang et al. [26] conducted a comprehensive study on ZnO and TiO_2, focusing on their UV-blocking capabilities while maintaining transparency. There are studies analyzing the efficiency of TiO_2 to reduce the photoaging of thermally treated bamboo [27] and wood surfaces [28,29] and studies on ZnO films deposited on wood surfaces [30], namely evaluating the hydrophobic and UV resistance properties of this thin film system [31]. These findings reveal that both materials exhibit robust UV-blocking properties, effectively safeguarding materials from the harmful effects of UV light exposure. Significantly, it has been observed that these two materials exhibit distinct differences in their band gap energies, a characteristic with critical implications for their performance. Specifically, TiO_2 exhibits a band gap energy ranging from 3.4 eV to 3.95 eV [32,33], while ZnO possesses a lower band gap energy, falling within the range of 3.1 eV to 3.3 eV [34,35]. These findings

conclusively establish that ZnO thin films possess a lower band gap energy compared to TiO_2, and this distinction holds significant ramifications for their respective effectiveness in safeguarding materials and their properties within challenging environments.

Coating cork material comes with its own set of challenges. Cork is highly deformable and sensitive to temperature changes, which demands a coating that is both flexible and adhesive. Moreover, cork surfaces are quite rough, and traditional polishing methods cannot be applied due to cork's cellular microstructure. Nevertheless, in a previous study [36], we successfully addressed these challenges by applying thin films of titanium dioxide (TiO_2) to cork substrates using magnetron sputtering (MS) and atomic layer deposition (ALD). The aim of the present work is to compare the effectiveness of TiO_2 and ZnO coatings prepared by MS in safeguarding cork material against harmful UV light exposure.

2. Materials and Methods

Two distinct deposition chambers, operated in DC mode, were employed to deposit TiO_2 and ZnO films. ZnO coatings were deposited using reactive magnetron sputtering within a customized EVA chamber [37] (Alliance Concept, Annecy, France) and TiO_2 films were deposited in a Teer chamber (Worcestershire, UK). The selection of different chambers and different conditions for different systems was linked to the dimensions of the respective targets (Table 1) as well as the characteristics and properties of Zn and Ti. Zn exhibits a melting point approximately 2.8 times lower than that of Ti (692.7 K and 1941 K at atmospheric pressure, respectively) and the sputtering yield, at 600 eV, of Zn surpasses that of Ti by a factor of 4.25. These fundamental differences in the melting point and sputtering yield strongly suggest shorter deposition times when depositing ZnO.

Table 1. Deposition parameters of TiO_2 and ZnO thin films.

Films	TiO₂	ZnO
Holder rotation (rpm)	12	0 (static)
Distance target-substrate (cm)	20	7
Base pressure ($\times 10^{-6}$ mbar)	15	2.5
Target surface dimension	38 cm $\times$ 17.5 cm	20 cm $\times$ 10 cm
Ar flow (sccm)	20	25
O₂ flow (sccm)	15	17
Working pressure (10^{-3} mbar)	1.7	5
Current (A)	6.27	1
Voltage (V)	430 ± 5	336 ± 3
Deposition time (min)	60	10

In addition to these considerations, the deposition rate of Ti decreases drastically due to target poisoning. The deposition rate of TiO_2 was also significantly lower, because the deposition was carried out in rotation mode. The adoption of rotation mode serves the purpose of minimizing the temperature elevation of substrates, a consequence of the higher current density associated with the Ti target (approximately 94 A/m^2 compared to 50 A/m^2 for the Zr target).

The films were deposited onto transparent Normax glass (76 mm $\times$ 76 mm $\times$ 1 mm) and cork sheets (30 mm $\times$ 20 mm $\times$ 1 mm) supplied by Amorim Cork Composites (Portugal). The cork sheets were created using cork granules ranging in size from 0.5 mm to 2 mm, blended with a polyurethane binder at a concentration of 6% by weight. The glass substrates underwent a meticulous cleaning process, involving sequential ultrasonic immersion in liquids: 15 min in ethanol, followed by 15 min in distilled water, and a subsequent 15 min in acetone. It is crucial to note that intentional heating of the substrates did not occur during the film deposition process. The specific deposition conditions for each type of film are comprehensively outlined in Table 1, providing a detailed summary of the procedural parameters employed in the replication of each sample set.

Morphological characterization of the coatings was conducted by means of scanning electron microscopy (SEM) in a Philips FEG-XL30s and a FEI Quanta 400 FEG ESEM microscopes (Amsterdam, Netherlands) operating at 3 and 10 kV, respectively. The SEM cross-sectional analysis was conducted by cutting and cleavage the coated glass sample and capturing post-sectioning images. Structural assessment was carried out using X-ray diffraction (XRD) operating in a Bragg–Brentano configuration with an EMPYREAN X-ray diffractometer (Malvern Panalytical, Malvirn, United Kingdom) equipped with a CuK_α X-ray source. Crystallite size (D) was estimated using Scherrer's equation [38,39]:

$$D = \frac{0.9\lambda}{\beta cos\theta} \tag{1}$$

where λ is the wavelength of the X-ray radiation, and θ and β are the position and broadening of the (002) ZnO peak obtained by fitting to a Lorentzian function. Optical transmittance measurements were performed using a Shimadzu UV-3101 PC spectrophotometer (Kyoto, Japan) covering wavelengths from 250 nm to 850 nm. Optical band gap energy of all the films was calculated using Tauc's law, considering that both films show a direct band gap [40]:

$$(\alpha h\nu)^2 = B\left(h\nu - E_g\right) \tag{2}$$

where B is a constant dependent on the material under investigation, $h\nu$ is the photon energy, E_g is the band gap energy, and α is the absorption coefficient which was calculated using the following equation [41]:

$$\alpha = \frac{2.303A}{d} \tag{3}$$

where d and A are the thickness and absorbance of the film, respectively.

The exposure test employed a sun simulator lamp. The global intensity of the light measured at the place where the samples were positioned was 2400 W/m^2. This comprehensive test spanned a duration of 68 h, which is roughly equivalent to the solar exposure received over 20 typical sunny days in Europe during the summer season [42]. To ensure rigorous testing conditions, we strategically positioned the coated and uncoated cork pieces in an area where the light intensity was at its maximum. Additionally, we included uncoated cork specimens under uncoated and ZnO-coated glass to evaluate the protective capabilities of a ZnO film not deposited on cork.

Color measurements of all the samples were conducted using a Minolta CM-2600d portable spectrophotometer (Tokyo, Japan) within the wavelength range of 360–700 nm to quantify their color coordinates (L^*, a^*, b^*) in accordance with the CIELab 1976 color space. Three different samples were measured per condition, and 5 measurements were carried out for each sample. The color variation (ΔC) of all the samples vs. the color of the original cork reference (L_R^*, a_R^*, b_R^*) was calculated using the following equation [36,43–45]:

$$\Delta C = \sqrt{\left(L^* - L_R^*\right)^2 + \left(a^* - a_R^*\right)^2 + \left(b^* - b_R^*\right)^2} \tag{4}$$

3. Results and Discussion

Figure 1 displays cross-sectional SEM images of the thin films deposited on glass substrates. Both films exhibit a remarkable density, resulting in a uniformly flat and smooth surface. Furthermore, the films exhibit homogeneity, marked by their compact structure and the absence of any discernible cracks or voids. The ZnO films show columnar growth. The micrographs of Figure 1 also depict the thicknesses of the films. Measurements performed at different points in the films' cross section revealed an average thickness of 52 ± 0 nm for TiO$_2$ and 399 ± 0.8 nm for ZnO. The reason for this remarkable difference lies in the rotating deposition mode of TiO$_2$ films and the low sputtering rate of the Ti target working in the poisoned mode.
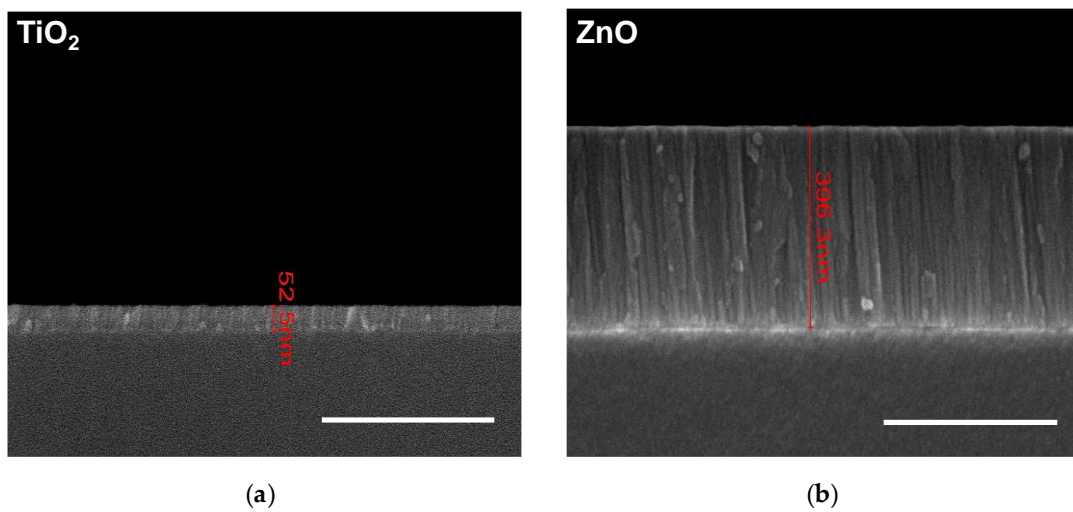
Figure 1. Scanning electron microscopy cross-sectional images of TiO$_2$ (**a**) and ZnO (**b**) thin films on glass substrates. Scale bars represent 500 nm.

The XRD patterns of the TiO$_2$ and ZnO thin films deposited on glass are depicted in Figure 2. A logarithmic intensity was plotted to highlight the presence of peaks of low intensity. Nevertheless, XRD analysis did not reveal any discernible peaks associated with TiO$_2$ reflections, which indicates that the TiO$_2$ film likely exhibits an amorphous structure. In contrast, the XRD pattern for the ZnO film exhibited two distinct peaks indexed as (002) and (004), in accordance with the ICCD card 01-079-0205 (hexagonal ZnO wurtzite structure with a P6$_3$mc space group). The absence of any other ZnO peak indicates a strong preferential orientation on the (002) direction, in line with the columnar growth observed by SEM. The average crystallite size calculated using Scherrer's equation was approximately 36 nm.
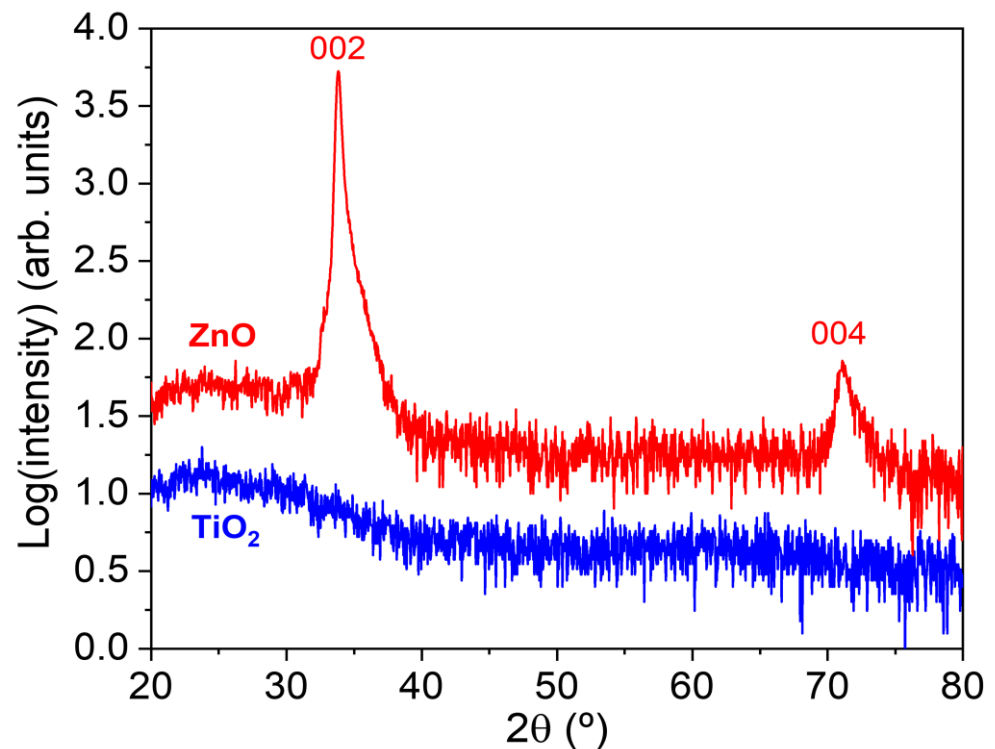

Figure 2. XRD patterns of TiO$_2$ and ZnO thin films on glass substrates. The Miller indexes of the peaks are included.

The optical transmittance spectra of both TiO$_2$ and ZnO films are illustrated in Figure 3a. It is evident from the graph that these layers exhibit transparency within the visible region of these spectra ($\lambda > 310$ nm for TiO$_2$ films and $\lambda > 370$ nm for ZnO films). Notably, within this visible spectrum, ZnO films demonstrate a slightly higher transparency (>80%) compared to TiO$_2$. The absorption edge of TiO$_2$, at 310 nm (≈ 4 eV), is located at notably lower wavelength than that of ZnO, which is located at 370 nm (≈ 3.35 eV). Consequently, both films possess the capacity to block a portion of UV radiation, although ZnO can filter a higher range.
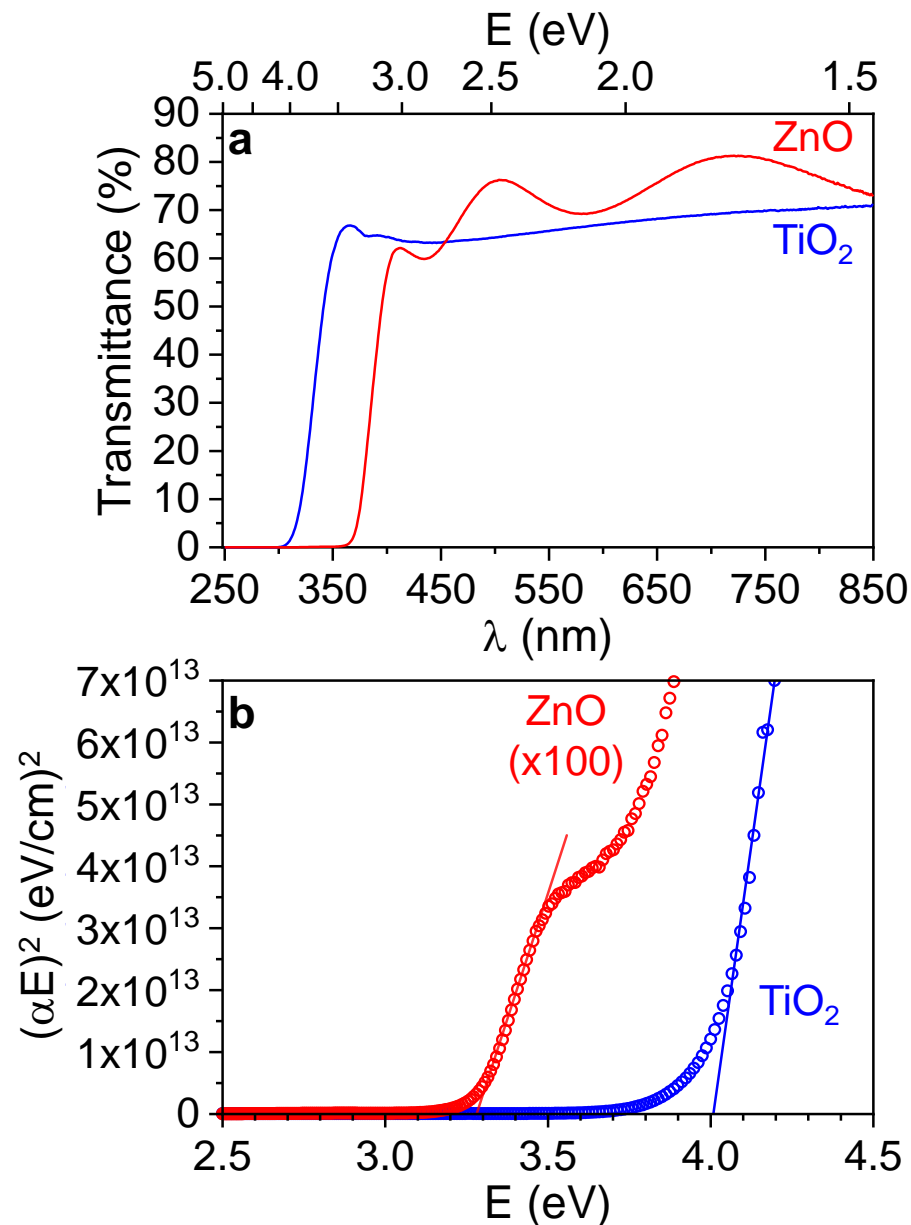

Figure 3. (**a**) Transmittance spectra of TiO$_2$ and ZnO thin films. (**b**) Tauc's plots for the direct band gap for both coatings.

Based on Tauc's equation (Equation (1)), the absorption coefficient was used to construct a plot, depicting ($\alpha h\nu$)^2 as a function of photon energy hν, illustrated in Figure 3b. The estimation of the optical band gap energy (E_g) was derived from the intersection point of the resulting linear regressions with the energy axis at ($\alpha h\nu$)$^2 = 0$. These calculations yielded direct band gap energy values of 4.00 eV for the amorphous TiO$_2$ films and 3.28 eV

for the ZnO film, which are very close to the values obtained directly from the transmittance spectra and are in good agreement with the literature [20–23].

Figure 4 presents a comprehensive analysis of the color coordinates (L^*, a^*, and b^*) of uncoated (alone and under glass) and coated (TiO$_2$ and ZnO) cork samples before and after exposure to the sun simulator for 68 h. The measurement of color variation (ΔC, see Equation (4)) in comparison to the unexposed cork reference is also included. At the top of Figure 4, the pictures of all the exposed and unexposed samples are presented for visual reference. As anticipated, the color coordinates of the unprotected cork (represented by the grey bars) exhibit noticeable alterations when compared to the unexposed cork ($\Delta C \sim 6$). This change corresponds to the discoloration observed by the naked eye, and it is corroborated by the visual depiction of the exposed samples in Figure 4. Remarkably, even higher color variations are observed for the exposed cork located under a glass piece ($\Delta C \sim 8$). The color differences observed in these samples further substantiate the discoloration due to exposure to UV, mainly caused by a large reduction in a^* (green–red chromaticity axis) and increase in L^* (lighter color). The change in the b^* chromaticity coordinate (blue–yellow axis) is significantly lower. Further, this reveals that glass does not provide any effective protection against UV ageing for cork; in fact, it seems to exacerbates the outcome, making the discoloration even more pronounced.

After applying the coating, we observed that the TiO$_2$ thin film had a minimal impact on the color of cork ($\Delta C < 2$). In fact, the color difference cannot be detected with the naked eye (cf. images in Figure 4). In contrast, the deposition of the ZnO film significantly affected the color change in the cork ($\Delta C > 4$). This effect is attributed to interference phenomena within the ZnO material, which can also be noticed in the oscillations (interference fringes) observed in the transmittance spectrum of ZnO in Figure 3a. However, color variations induced by the deposition process (e.g., substrate heating under an O$_2$ atmosphere) cannot be discarded. The color change caused by ZnO is easily noticeable with the naked eye, as depicted in the images in Figure 4. After subjecting both coated samples to exposure under the sun simulator lamp, we observed a substantial color change in the samples coated with TiO$_2$, reaching $\Delta C > 8$. This variation is similar to that observed for uncoated cork (increase in b^* and L^* and reduction in a^*, leading to large values of ΔC), indicating that the TiO$_2$ film was ineffective as a UV blocker for cork. This change was highly noticeable with the naked eye, indicating significant damage to the cork sample. In contrast, the sample coated with ZnO demonstrated greater resistance to UV light. These samples exhibited only a slight color change compared to the ZnO-coated cork before exposure ($\Delta C < 0.5$). This difference is even more imperceptible when visually inspecting the samples; it is virtually impossible to detect any change between the unexposed and exposed ZnO-coated samples, as illustrated by the visual representations of the samples at the top of Figure 4. To discard the influence of the variations induced by the deposition of ZnO in the cork substrate, we also examined the color of a cork sample located under glass coated with ZnO during the same exposure period. In contrast to the uncoated glass piece, no discernible difference in color can be observed with the naked eye, as depicted in Figure 4. This negligible color variation was confirmed by the very small color difference compared with the uncoated substrate ($\Delta C \approx 1$). In fact, the three color coordinates remain almost identical to the original reference after 68 h of exposure under the sun simulator lamp. Consequently, the ZnO thin film emerges as an effective protector of cork material against UV light, while the TiO$_2$ film and glass do not provide substantial UV protection for cork. This outcome aligns with the optical characteristics of the films, since the ZnO thin film has the capacity to block UV light with a wavelength of up to 370 nm within the UV region. In addition, the higher thickness of the ZnO coating is another factor justifying its better UV-protective properties.
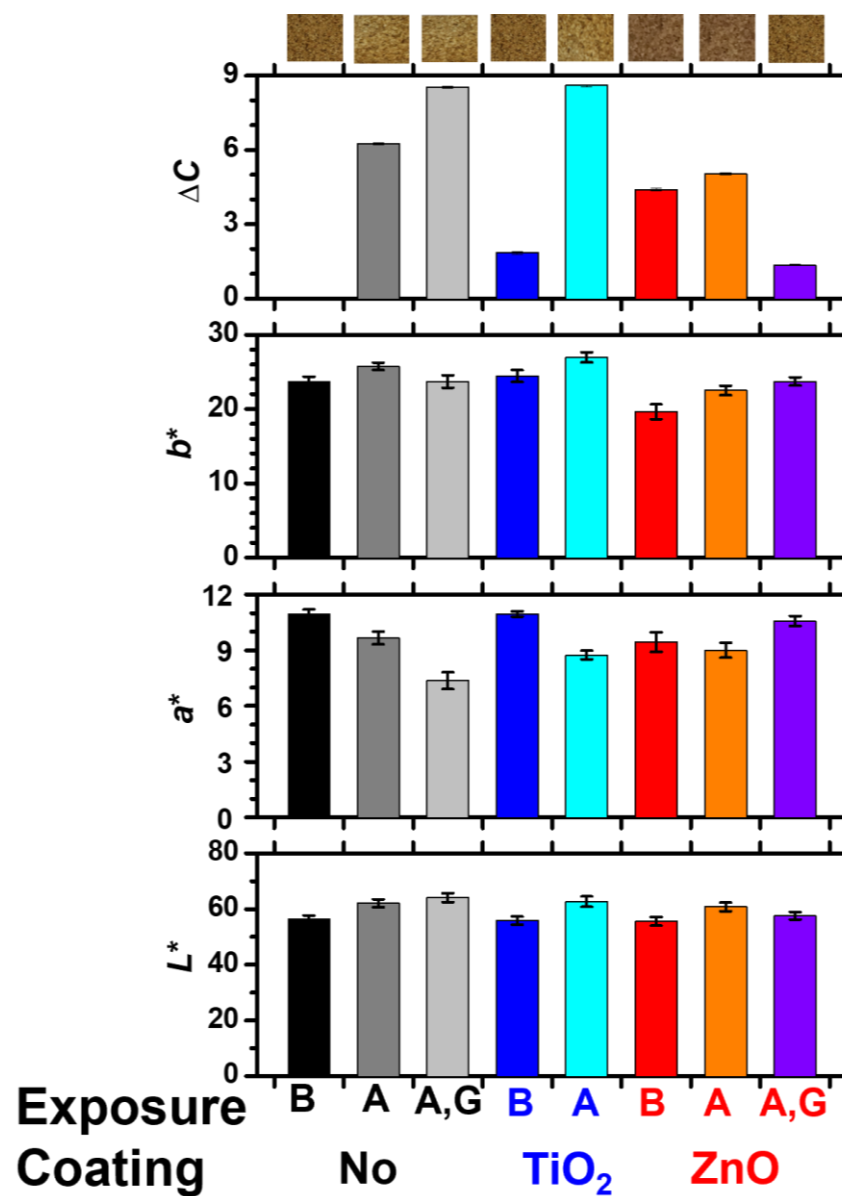
Figure 4. Color coordinates (*L**, *a**, and *b**) of uncoated and coated (TiO$_2$ and ZnO) cork before (B) and after (A) a 68 h exposure to a sun simulator lamp. Samples located under uncoated and ZnO-coated glass after exposure (A,G) are also included. The overall change in color (ΔC, as defined in Equation (4)) was assessed in comparison to the respective cork substrate with no exposure. Images of all the samples are included at the top of the figure.

4. Conclusions

TiO$_2$ and ZnO films were deposited on cork to provide protection against UV ageing. The deposited films exhibited remarkable uniformity and a smooth surface, with no discernible cracks or voids. Both films are transparent within the visible light range. The amorphous TiO$_2$ film can block UV light with a wavelength of up to 310 nm (with E_g = 4.00 eV), while the crystalline ZnO thin film can block UV light with a wavelength of up to 370 nm (with E_g = 3.28 eV).

Uncoated cork samples experienced significant color changes (damage) when exposed to sun simulator light for 68 h, even when located under a glass piece. The deposition of TiO$_2$ did not significantly influence the color of the cork, while ZnO induced a slightly larger color change, likely due to the interference phenomena of the film. However, TiO$_2$ failed to preserve the color of the cork after the sun exposure test. On the contrary, the

ZnO-coated cork did not display any important discoloration after the exposure test. The same was observed for cork located under glass coated with ZnO.

The failure of TiO_2 films to prevent cork discoloration probably arises from the lack of filtering of low-energy UV rays, but the impact of its lower thickness cannot be discarded. In contrast, ZnO appears to be a great alternative for efficiently protecting cork from discoloration caused by UV sunlight, thereby representing a viable solution to mitigate ageing. The application of this protective coating extends the versatility of cork materials, making them suitable for various practical uses, including outdoor and indoor flooring, walling materials, and also shoes, bags, and wallets. The resilience of ZnO-coated cork against UV-induced aging not only enhances this material's durability but also broadens its spectrum of potential applications across different settings.

References

1. Pereira, H. The Rationale behind Cork Properties: A Review of Structure and Chemistry. *BioResources* **2015**, *10*, 6207–6229. [CrossRef]
2. Silva, S.S.P.; Sabino, M.A.; Fernandes, E.M.; Correlo, V.M.; Boesel, L.F.; Reis, R.L. Cork: Properties, capabilities and applications. *Int. Mater. Rev.* **2005**, *50*, 345–365. [CrossRef]
3. Lequin, S.; Chassagne, D.; Karbowiak, T.; Simon, J.-M.; Paulin, C.; Bellat, J.-P. Diffusion of oxygen in cork. *J. Agric. Food Chem.* **2012**, *60*, 3348–3356. [CrossRef] [PubMed]
4. Pereira, H. *Cork: Biology, Production and Uses*; Elsevier Science: Amsterdam, The Netherlands, 2007.
5. Gil, L. New cork-based materials and applications. *Materials* **2015**, *8*, 625–637. [CrossRef] [PubMed]
6. Malhotra, A.; Abrol, M.; Shaji, J. Adapting Sustainable Materials for Interiors-Pre & Post Covid Scenarios and Applications. *Int. J. Eng. Res.* **2022**, *12*, 1–14.
7. Fortes, M.A.; Nogueira, M.T. The poison effect in cork. *Mater. Sci. Eng. A* **1989**, *122*, 227–232. [CrossRef]
8. Mateus, M.M.; Bordado, J.M.; dos Santos, R.G. Ultimate use of Cork–Unorthodox and innovative applications. *Ciênc. Tecnol. Mater.* **2017**, *29*, 65–72. [CrossRef]
9. Demertzi, M.; Garrido, A.; Dias, A.C.; Arroja, L. Environmental performance of a cork floating floor. *Mater. Des.* **2015**, *82*, 317–325. [CrossRef]
10. Sakraker, I.; Chazot, O.; Carvalho, J.P. Performance of cork-based thermal protection material P50 exposed to air plasma: An experimental study. *CEAS Space J.* **2022**, *14*, 377–393. [CrossRef]
11. Gibson, L.J.; Ashby, M.F. *Cellular Solids*; Cambridge University Press: Cambridge, UK, 1997.
12. Gil, L. Cork Composites: A Review. *Materials* **2009**, *2*, 776–789. [CrossRef]
13. Guo, A.R.; Li, J.; Xiao, D.H.; Liu, C. Preparation and Properties of Insulation Flexible Cork Composites. *Cailiao Gongcheng-J. Mater. Eng.* **2017**, *45*, 1–9. [CrossRef]
14. Kocáb, J.; Kottner, R.; Kossa, A. Characterization of a cork-rubber composite using advanced material models. *Mater. Today-Proc.* **2019**, *12*, 340–345. [CrossRef]
15. Lopes, H.; Silva, S.P.; Carvalho, J.P.; Machado, J. The Influence of Cork and Manufacturing Parameters on the Properties of Cork-Rubber Composites for Vibration Isolation Applications. *Sustainability* **2021**, *13*, 11240. [CrossRef]

16. Lopes, H.; Silva, S.P.; Machado, J. FEA Approach for Predicting the Dynamic Behaviour of Cork-Rubber Composites. *Int. J. Simul. Model.* **2022**, *21*, 237–248. [CrossRef]

17. Lopes, H.; Silva, S.P.; Machado, J. Analysis of the Effect of Shape Factor on Cork-Rubber Composites under Small Strain Compression. *Appl. Sci.* **2020**, *10*, 7177. [CrossRef]

18. Yoon, B.; Cho, S.H.; Lee, S.K.; Cho, K.; Tabe, C.A.; Giese, U.; Nam, J.D.; Suhr, J. Natural cork/potato periderm derivatives enabled interface engineering of elastomer composites for tunable energy-absorbing capabilities. *Ind. Crops Prod.* **2021**, *170*, 113763. [CrossRef]

19. Lanca, M.C.; Peuckert, S.; Neagu, E.R.; Gil, L.; Silva, P.C.; Marat-Mendes, J. Electrical Properties Studies of a Cork/TetraPak®/Paraffin Wax Composite. *Adv. Mater. Forum IV* **2008**, *587–588*, 613–617. [CrossRef]

20. Guo, L.; Huang, G.; Zheng, J.; Li, G. Thermal oxidative degradation of styrene-butadiene rubber (SBR) studied by 2D correlation analysis and kinetic analysis. *J. Therm. Anal. Calorim.* **2014**, *115*, 647–657. [CrossRef]

21. Romero-Sánchez, M.D.; Mercedes Pastor-Blas, M.; Martín-Martínez, J.M.; Walzak, M.J. Addition of ozone in the UV radiation treatment of a synthetic styrene-butadiene-styrene (SBS) rubber. *Int. J. Adhes. Adhes.* **2005**, *25*, 358–370. [CrossRef]

22. Yousefi, F.; Mousavi, S.B.; Heris, S.Z.; Naghash-Hamed, S. UV-shielding properties of a cost-effective hybrid PMMA-based thin film coatings using TiO_2 and ZnO nanoparticles: A comprehensive evaluation. *Sci. Rep.* **2023**, *13*, 7116–7134. [CrossRef]

23. Melvin Ng, H.K.; Leo, C.P. Translucent and adsorptive PVA thin film containing microfibrillated cellulose intercalated with TiO_2 nanoparticles for dye removal. *Colloids Surf. A Physicochem. Eng.* **2019**, *578*, 123590–123598.

24. Zhang, Z.; Zhang, B.; Grishkewich, N.; Berry, R.; Tam, K.C. Cinnamate-functionalized cellulose nanocrystals as UV-shielding nanofillers in sunscreen and transparent polymer films. *Adv. Sustain. Syst.* **2019**, *3*, 1800156–1800160. [CrossRef]

25. Johansson, W.; Peralta, A.; Jonson, B.; Anand, S.; Österlund, L.; Karlsson, S. Transparent TiO_2 and ZnO thin films on glass for UV protection of PV modules. *Front. Mater.* **2019**, *6*, 259–268. [CrossRef]

26. Yang, D.; Ramu, A.G.; Choi, D. Synthesis of Transparent ZnO–TiO_2 and Its Nanocomposites for Ultraviolet Protection of a Polyethylene Terephthalate (PET) Film. *Catalysts* **2022**, *12*, 1590. [CrossRef]

27. Tang, A.R.; Huang, Y.Q.; Zhang, W.; Yu, Y.; Yang, Y.; Yuan, Z.R.; Wang, X.Z. Effect of the nano-titanium dioxide (nano-TiO_2) coating on the photoaging properties of thermally treated bamboo. *Wood Mater. Sci. Eng.* **2022**, *17*, 895–904. [CrossRef]

28. Jnido, G.; Ohms, G.; Viöl, W. One-Step Deposition of Polyester/TiO_2 Coatings by Atmospheric Pressure Plasma Jet on Wood Surfaces for UV and Moisture Protection. *Coatings* **2020**, *10*, 184. [CrossRef]

29. Jnido, G.; Ohms, G.; Viöl, W. Deposition of TiO_2 Thin Films on Wood Substrate by an Air Atmospheric Pressure Plasma Jet. *Coatings* **2018**, *9*, 441. [CrossRef]

30. Jnido, G.; Ohms, G.; Viöl, W. Deposition of Zinc Oxide Coatings on Wood Surfaces Using the Solution Precursor Plasma Spraying Process. *Coatings* **2021**, *11*, 183. [CrossRef]

31. Wang, Y.N.; Wu, X.T.; Wang, Y.B.; Tian, Y.Q.; Mu, H.B.; Li, J.K. Hydrophobic and UV-resistant properties of environmentally friendly nano-ZnO-coated wood. *Holzforschung* **2021**, *75*, 138–147. [CrossRef]

32. Al-Shomar, S.M.; Alahmad, W.R. Annealing temperature effect on structural, optical and photocatalytic activity of nanocrystalline TiO_2 films prepared by sol-gel method used for solar cell application. *Dig. J. Nanomater. Biostruct.* **2019**, *14*, 617–625.

33. Guang-Lei, T.; Hong-Bo, H.E.; Jian-Da, S. Effect of microstructure of TiO_2 thin films on optical band gap energy. *Chin. Phys. Lett.* **2005**, *22*, 1787–1789. [CrossRef]

34. Wasan, R.S.; Nada, M.S.; Wesam, A.T.; Mohammed, A. Synthesis sol-gel derived highly transparent ZnO thin films for optoelectronic applications. *Adv. Mater. Phys. Chem.* **2012**, *2012*, 17891–17896.

35. Najim, S.A.; Alyas, M.M.; Sulaiman, A.A. Structural and optical properties of copper-doped ZnO thin films at different weight percentage. *Dig. J. Nanomater. Biostructures* **2022**, *17*, 677–683. [CrossRef]

36. Martínez-Martínez, D.; Tiss, B.; Glanzmann, L.N.; Wolthuizen, D.J.; Cunha, L.; Mansilla, C.; De Hosson, J.T.M. Protective films on complex substrates of thermoplastic and cellular elastomers: Prospective applications to rubber, nylon and cork. *Surf. Coat. Technol.* **2022**, *442*, 128405–128415. [CrossRef]

37. Cooke, K.E.; Bamber, M.; Bassas, J.; Boscarino, D.; Derby, B.; Figueras, A.; Inkson, B.J.; Rigato, V.; Steer, T.; Teer, D.G. Multilayer nitride coatings by closed field unbalanced magnetron sputter ion plating. *Surf. Coat. Technol.* **2003**, *162*, 276–287. [CrossRef]

38. Scherrer, P. Bestimmung der Größe und der inneren Struktur von Kolloidteilchen mittels Röntgenstrahlen. *Nach Ges Wiss Gottingen* **1918**, *2*, 8–100.

39. Patterson, A. The Scherrer Formula for X-ray Particle Size Determination. *Phys. Rev.* **1939**, *56*, 978–982. [CrossRef]

40. Tauc, J. Optical properties and electronic structure of amorphous Ge and Si. *Mater. Res. Bull.* **1968**, *3*, 37–46. [CrossRef]

41. Tiss, B.; Benfraj, M.; Bouguila, N.; Kraini, M.; Alaya, S.; Cristea, D.; Croitoru, C.; Craciun, V.; Craciun, D.; Prepelita, P.; et al. The effect of vacuum and air annealing in the physical characteristics and photocatalytic efficiency of In_2S_3: Ag thin films produced by spray pyrolysis. *Mater. Chem. Phys.* **2021**, *270*, 124838–124849. [CrossRef]

42. Handara, V.A.; Illya, G.; Tippabhotla, S.K.; Shivakumar, R.; Budiman, A.S. Center for Solar Photovoltaics (CPV) at Surya University: Novel and Innovative Solar Photovoltaics System Designs for Tropical and Near-Ocean Regions (An Overview and Research Directions). *Procedia Eng.* **2016**, *139*, 22–31. [CrossRef]

43. Wyszecki, G.; Stiles, W.S. *Color Science—Concepts and Methods, Quantitative Data and Formulas*; Wiley: New York, NY, USA, 1967.

44.   Judd, D.B.; Wyszecki, G. *Color in Business, Science and Industry*; Wiley: New York, NY, USA, 1975.
45.   Mcdonald, R. *Colour Physics for Industry*; Society of Dyers and Colourists: Bradford, UK, 1987.